Supplementary Material for Analytic Marching: An Analytic Meshing Solution from Deep Implicit Surface Networks

Jiabao Lei [1 2] **Kui Jia** [1 2]

1. Proof of Theorem 5

Proof. The proof proceeds by first showing that each planar face on the surface $\mathcal{Z}$ captured by the SDF $F = f \circ \boldsymbol{T}$ uniquely corresponds to an analytic face of an analytic cell, and then showing that for any pair of planar faces connected on $\mathcal{Z}$, their corresponding analytic faces are connected via boundaries of their respective analytic cells.

Let $\mathcal{P}_1$ denote a planar face on the surface $\mathcal{Z}$, and $\boldsymbol{n}_1 \in \mathbb{R}^3$ be its normal. We have $\boldsymbol{n}_1^\top \boldsymbol{x} = 0 \ \forall \ \boldsymbol{x} \in \mathcal{P}_1$. Equation (8) tells that $\boldsymbol{n}_1$ must be proportional at least to one of $\{\boldsymbol{a}_F^r | r \in \mathcal{R}\}$. By the unique plane condition, i.e., each of $\{\boldsymbol{a}_F^r | r \in \mathcal{R}\}$ is uniquely defined, we have $\boldsymbol{n}_1 \propto \boldsymbol{a}_F^{r_1 \top}$ of a certain region r_1. Assume r_1 is not an analytic cell, which suggests that there exists no intersection between $\boldsymbol{a}_F^{r_1}$ and r_1 and we have $\boldsymbol{a}_F^{r_1} \boldsymbol{x} = \boldsymbol{n}_1^\top \boldsymbol{x} \neq 0$ for all $\boldsymbol{x} \in r_1$, and thus $\mathcal{P}_1 \wedge r_1 = \emptyset$; it suggests that the normal $\boldsymbol{n}_1$ of $\mathcal{P}_1$ is induced in a different region r_1' by $\boldsymbol{n}_1 \propto \boldsymbol{a}_F^{r_1'} = \boldsymbol{w}_f^\top \boldsymbol{T}^{r_1'}$, which contradicts with the assumed unique plane condition. We thus have that r_1 must be an analytic cell.

Let $\boldsymbol{n}_1 \propto \boldsymbol{a}_F^{\tilde{r}_1 \top}$ of a certain analytic cell $\tilde{r}_1 \in \widetilde{\mathcal{R}}$ (or $\mathcal{C}_F^{\tilde{r}_1}$), and we have the analytic face $\mathcal{P}_F^{\tilde{r}_1} \subseteq \mathcal{P}_1$. Assume there exist $\mathcal{P}_1 - \mathcal{P}_F^{\tilde{r}_1} = \{\boldsymbol{x} \in \mathcal{Z} | \boldsymbol{x} \in \mathcal{P}_1, \boldsymbol{x} \notin \mathcal{P}_F^{\tilde{r}_1}\}$, which means that for any $\boldsymbol{x} \in \mathcal{P}_1 - \mathcal{P}_F^{\tilde{r}_1}$, it resides in an analytic face $\mathcal{P}_F^{\tilde{r}_1'}$ of a different cell $\mathcal{C}_F^{\tilde{r}_1'}$; since $\boldsymbol{x} \in \mathcal{P}_1$, we have $\boldsymbol{n}_1 \propto \boldsymbol{a}_F^{\tilde{r}_1' \top}$ and thus $\boldsymbol{a}_F^{\tilde{r}_1} \propto \boldsymbol{a}_F^{\tilde{r}_1'}$, which contradicts with the unique plane condition of $\boldsymbol{a}_F^{\tilde{r}_1} \not\propto \boldsymbol{a}_F^{\tilde{r}_1'}$. We thus have $\mathcal{P}_1 = \mathcal{P}_F^{\tilde{r}_1}$ and $\mathcal{P}_1 \subset \mathcal{C}_F^{\tilde{r}_1}$. By the definition (12) of analytic face, the above argument also tells that planar faces on $\mathcal{Z}$ and analytic faces $\{\mathcal{C}_F^{\tilde{r}} | \tilde{r} \in \widetilde{\mathcal{R}}\}$ are one-to-one corresponded.

Assume $\mathcal{P}_1$ connects with another planar face $\mathcal{P}_2$ on a shared edge segment $\mathcal{E} = \{\boldsymbol{x} \in \mathcal{Z} | \boldsymbol{x} \in \mathcal{P}_1, \boldsymbol{x} \in \mathcal{P}_2\}$. Define

the normal of $\mathcal{P}_2$ as $\boldsymbol{n}_2 \in \mathbb{R}^3$, we have $\boldsymbol{n}_1 \not\propto \boldsymbol{n}_2$. Let $\mathcal{P}_2 \subset \mathcal{C}_F^{\tilde{r}_2}$, and we thus have $\mathcal{E} \subset \mathcal{C}_F^{\tilde{r}_1}$ and $\mathcal{E} \subset \mathcal{C}_F^{\tilde{r}_2}$, which tells that the two cells $\mathcal{C}_F^{\tilde{r}_1}$ and $\mathcal{C}_F^{\tilde{r}_2}$ connect at least on $\mathcal{E}$. Due to the monotonous and convex nature of linear analytic cells $\{\mathcal{C}_F^{\tilde{r}} | \tilde{r} \in \widetilde{\mathcal{R}}\}$, $\mathcal{E}$ must be on the boundaries of both $\mathcal{C}_F^{\tilde{r}_1}$ and $\mathcal{C}_F^{\tilde{r}_2}$, and the boundaries of $\mathcal{C}_F^{\tilde{r}_1}$ and $\mathcal{C}_F^{\tilde{r}_2}$ share at least on $\mathcal{E}$. There exist two cases for the connection of cell boundaries on $\mathcal{E}$: (1) in the general case, $\mathcal{C}_F^{\tilde{r}_1}$ and $\mathcal{C}_F^{\tilde{r}_2}$ share a boundary $\mathcal{B}_F^{\tilde{r}_1 \tilde{r}_2}$ defined by a hyperplane $H_{lk}^{\tilde{r}_1 \tilde{r}_2} = \{\boldsymbol{x} \in \mathbb{R}^3 | \boldsymbol{a}_{lk}^{\tilde{r}_1 \tilde{r}_2} \boldsymbol{x} = 0\}$, and we have $\mathcal{E} \in \mathcal{B}_F^{\tilde{r}_1 \tilde{r}_2}$, which, based on Corollary 4 and Definition 2, suggests that the two cells have a switching neuron state $s_{lk}(\boldsymbol{x}) \ \forall \ \boldsymbol{x} \in \mathcal{B}_F^{\tilde{r}_1 \tilde{r}_2}$, and consequently a switching neuron state $s_{lk}(\boldsymbol{x}) \ \forall \ \boldsymbol{x} \in \mathcal{E}$; (2) in some rare case, $\mathcal{E}$ coincides with a cell edge of $\mathcal{C}_F^{\tilde{r}_1}$ defined by $\{\boldsymbol{x} \in \mathbb{R}^3 | \boldsymbol{a}_{l_1 k_1}^{\tilde{r}_1} \boldsymbol{x} = 0, \boldsymbol{a}_{l_1' k_1'}^{\tilde{r}_1} \boldsymbol{x} = 0\}$, and a cell edge of $\mathcal{C}_F^{\tilde{r}_2}$ defined by $\{\boldsymbol{x} \in \mathbb{R}^3 | \boldsymbol{a}_{l_2 k_2}^{\tilde{r}_2} \boldsymbol{x} = 0, \boldsymbol{a}_{l_2' k_2'}^{\tilde{r}_2} \boldsymbol{x} = 0\}$, and it is not necessary that $l_1 k_1$ and $l_2 k_2$ specify the same neuron, and $l_1' k_1'$ and $l_2' k_2'$ specify another same neuron. Due to a phenomenon similar to the blessing of (high) dimensionality (Gorban & Tyukin, 2018), the second case of coincidence is expected to happen with a low probability. In any of the two cases, the boundaries $\mathcal{C}_F^{\tilde{r}_1}$ and $\mathcal{C}_F^{\tilde{r}_2}$ respectively associated with $\mathcal{P}_1$ and $\mathcal{P}_2$ connect on $\mathcal{E}$.

Since for any pair of planar faces $\mathcal{P}_1$ and $\mathcal{P}_2$ connected on $\mathcal{Z}$, we prove that they are uniquely corresponded to a pair of analytic faces $\mathcal{P}_F^{\tilde{r}_1}$ and $\mathcal{P}_F^{\tilde{r}_2}$, which are connected via boundaries of their respective analytic cells $\mathcal{C}_F^{\tilde{r}_1}$ and $\mathcal{C}_F^{\tilde{r}_2}$. The theorem is proved. $\square$

2. More qualitative results

We show additional qualitative results for the categories of "Airplane", "Rifle", "Chair", and "Table" in Figures 1, 2, 3, and 4. To help understand the polygonal mesh produced by analytic marching, we further zoom in the focused area of our "Sofa" result reported in Figure 3 of the main text, and show the zoomed result in Figure 5. Note that the polygonal mesh produced by analytic marching can be easily converted as triangle mesh, simply by connecting diagonals on individual polygonal faces.
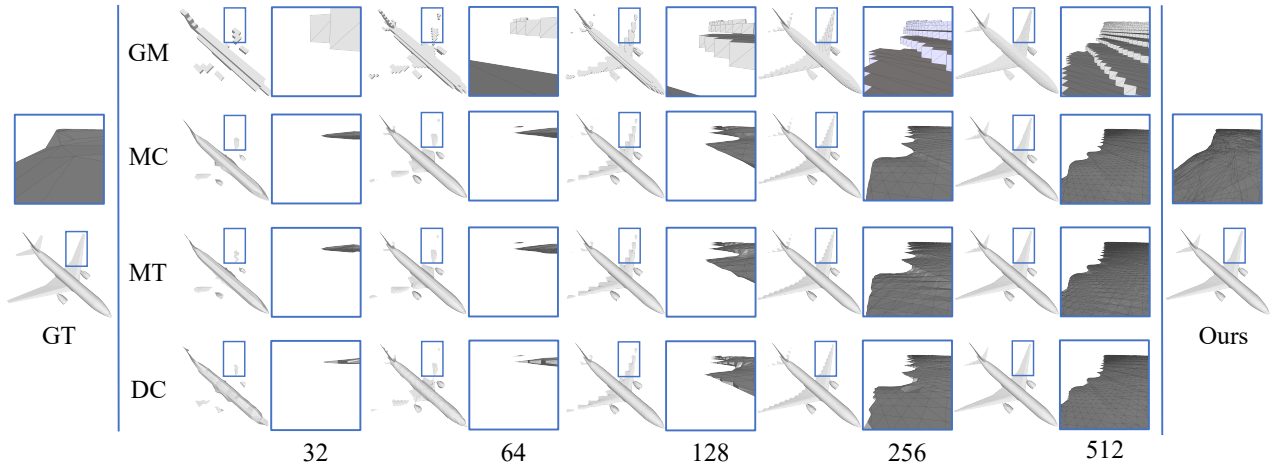

Figure 1. Qualitative comparisons of different meshing algorithms. For greedy meshing (GM), marching cubes (MC), marching tetrahedra (MT), and dual contouring (DC), results under a resolution range of discrete point sampling from 32^3 to a GPU memory limit of 512^3 are presented.
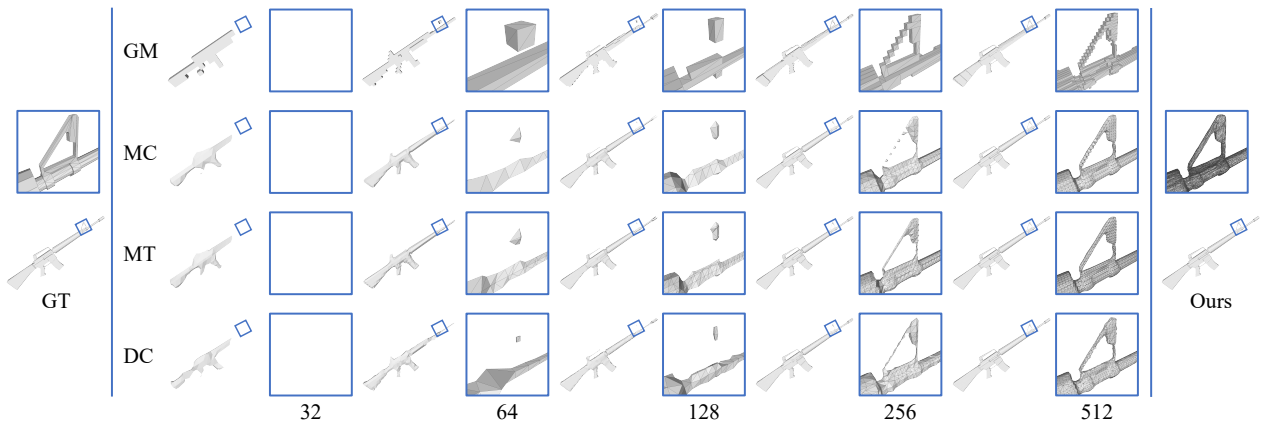

Figure 2. Qualitative comparisons of different meshing algorithms. For greedy meshing (GM), marching cubes (MC), marching tetrahedra (MT), and dual contouring (DC), results under a resolution range of discrete point sampling from 32^3 to a GPU memory limit of 512^3 are presented.

3. Numerical results

We show in Table 1 the numerical results corresponding to the plotted curves in Figure 2 of the main text.
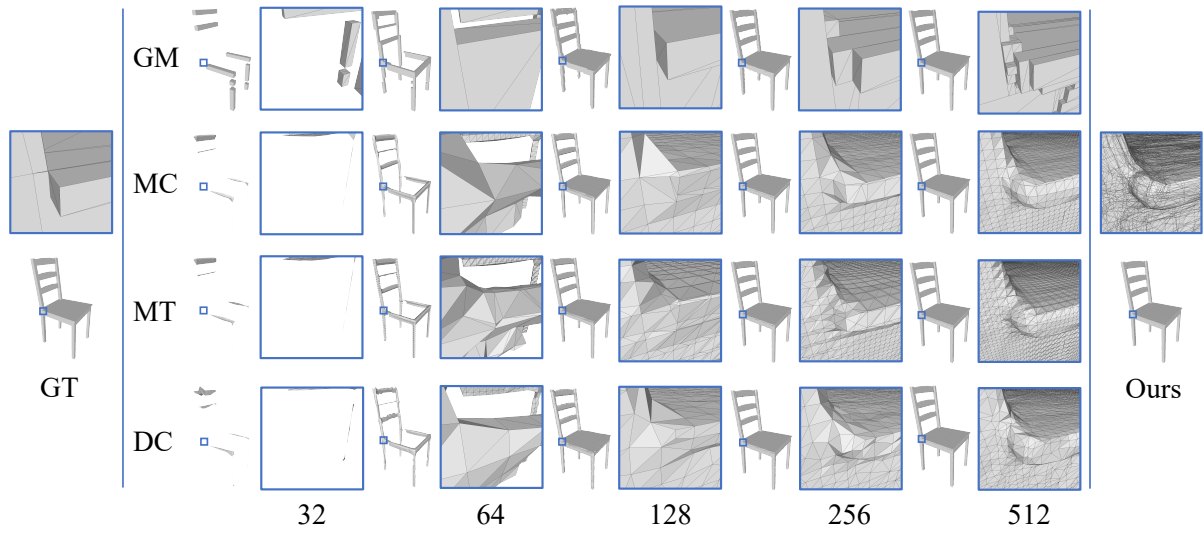
Figure 3. Qualitative comparisons of different meshing algorithms. For greedy meshing (GM), marching cubes (MC), marching tetrahedra (MT), and dual contouring (DC), results under a resolution range of discrete point sampling from 32^3 to a GPU memory limit of 512^3 are presented.
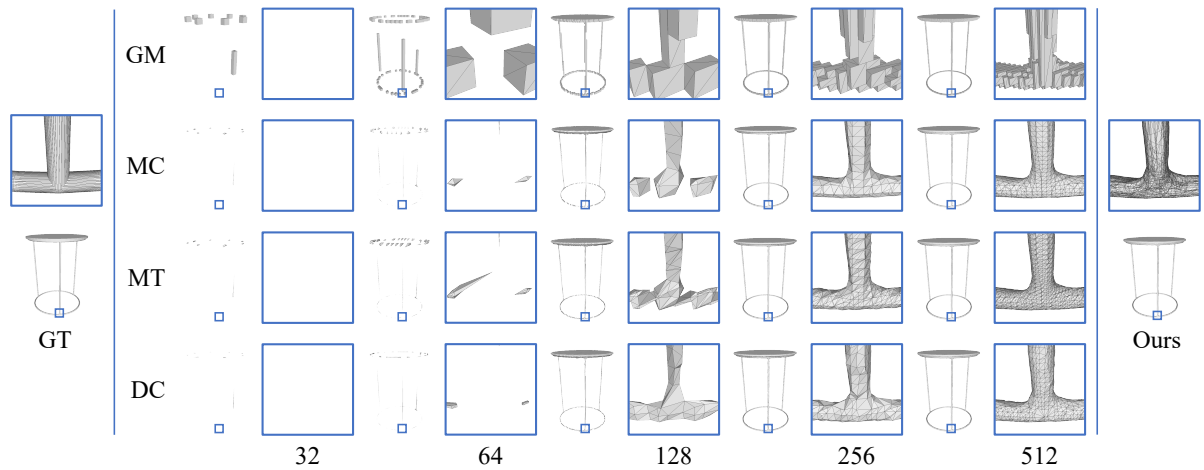

Figure 4. Qualitative comparisons of different meshing algorithms. For greedy meshing (GM), marching cubes (MC), marching tetrahedra (MT), and dual contouring (DC), results under a resolution range of discrete point sampling from 32^3 to a GPU memory limit of 512^3 are presented.

Figure 5. A local surface area of the polygonal mesh produced by analytic marching, which is obtained by further zooming in the focused area of our "Sofa" result reported in Figure 3 of the main text. *Note that the polygonal mesh produced by analytic marching can be easily converted as triangle mesh, simply by connecting diagonals on individual polygonal faces.*

Table 1. Numerical results of different meshing algorithms under metrics of recovery precision and inference world-clock time. For greedy meshing (GM), marching cubes (MC), marching tetrahedra (MT), and dual contouring (DC), results under a resolution range of discrete point sampling from 32^3 to a GPU memory limit of 512^3 are presented, and the dominating computations of their sampled points' SDF values are implemented on GPU.

Algorithms	CD($\times 10^{-1}$)	EMD($\times 10^{-3}$)	IoU(%)	F@τ(%)	F@2τ(%)	Time(sec.)
MC32	37.280	25.368	72.266	39.805	78.332	2.25
MC64	6.4457	8.8759	88.461	61.098	96.116	2.41
MC128	5.5740	6.7293	91.348	66.585	97.194	3.41
MC256	5.5731	6.5415	91.410	66.773	97.202	14.0
MC512	5.5730	6.5403	91.445	66.777	97.205	156
GM32	45.599	23.918	63.356	19.725	55.441	2.41
GM64	11.006	11.259	76.122	32.580	88.112	2.50
GM128	6.8142	8.0922	85.078	53.570	96.793	3.40
GM256	5.9424	6.9674	88.446	63.411	97.008	14.2
GM512	5.7248	6.7480	90.098	65.548	97.015	171
MT32	38.485	25.383	73.677	41.673	79.961	2.62
MT64	6.5388	8.8540	88.628	61.548	96.088	3.47
MT128	5.6575	6.6818	91.306	66.691	97.228	7.33
MT256	5.5276	6.6185	91.335	66.994	97.236	29.5
MT512	5.5109	6.6117	91.347	66.995	97.239	204
DC32	41.570	28.735	70.134	37.162	74.564	2.46
DC64	6.9833	9.9407	87.627	59.704	95.506	2.61
DC128	5.6615	6.7204	91.304	66.562	97.215	3.76
DC256	5.5449	6.6735	91.349	66.921	97.220	16.2
DC512	5.5421	6.6165	91.355	66.927	97.221	177
Ours	5.5049	6.5401	91.451	67.153	97.239	20.8